

# Electrochemical Study and Modeling of H<sub>2</sub>S Corrosion of Mild Steel

Yougui Zheng,<sup>†,\*</sup> Bruce Brown,<sup>\*</sup> and Srdjan Nešić<sup>\*</sup>

## ABSTRACT

The internal corrosion of mild steel in the presence of hydrogen sulfide (H<sub>2</sub>S) represents a significant challenge in oil production and natural gas treatment facilities, but the underlying mechanisms involved in H<sub>2</sub>S corrosion are still not fully understood. This lack of knowledge makes the prediction, prevention, and/or control of aqueous H<sub>2</sub>S corrosion of mild steel much more difficult. In the present study, H<sub>2</sub>S corrosion mechanisms were experimentally investigated in short-term corrosion tests (lasting 1 h to 2 h), conducted in a 1 wt% sodium chloride (NaCl) solution at different pH (pH 2 to pH 5), at different temperatures (30°C to 80°C), under various H<sub>2</sub>S/N<sub>2</sub> gaseous concentration ratios (0 to 10%(v)) and flow rates, using a X65 mild steel rotating cylinder electrode. Corrosion rates were measured by linear polarization resistance (LPR). Corrosion mechanisms were investigated by using potentiodynamic sweeps and by comparison with electrochemical modeling. LPR results showed that corrosion rates increased with increasing temperature, partial pressure of H<sub>2</sub>S, flow rate, and decreasing pH. Results of potentiodynamic sweeps show the presence of H<sub>2</sub>S could affect both cathodic reactions and the anodic reaction. An electrochemical model was developed and can be used to predict the effect of temperature, pH, pH<sub>2</sub>S, and flow on corrosion mechanisms of mild steel in aqueous solutions containing H<sub>2</sub>S in the absence of protective iron sulfide layers.

**KEY WORDS:** carbon steel, corrosion rate, hydrogen sulfide, modeling, uniform corrosion

Submitted for publication: January 30, 2013. Revised and accepted: October 1, 2013. Preprint available online: October 17, 2013. doi: <http://dx.doi.org/10.5006/0937>.

<sup>†</sup> Corresponding author. E-mail: [yz175108@ohio.edu](mailto:yz175108@ohio.edu).

<sup>\*</sup> Institute for Corrosion and Multiphase Technology, Department of Chemical and Biomolecular Engineering, Ohio University, 342 W. State St., Athens, OH 45701.

## INTRODUCTION

The corrosion of mild steel by hydrogen sulfide (H<sub>2</sub>S)-containing media has been investigated since the 1940s.<sup>1</sup> Recently, more attention was focused on this type of corrosion because of harsher environments encountered when exploring new sources of oil and gas, which usually contain H<sub>2</sub>S. The understanding, prediction, and control of H<sub>2</sub>S corrosion are some of the big challenges in oil and gas production and transportation. Despite the relative abundance of experimental data on H<sub>2</sub>S corrosion of mild steel, most of the literature is still confusing and somewhat contradictory. Therefore, the mechanism of H<sub>2</sub>S corrosion remains much less understood when compared to that of carbon dioxide (CO<sub>2</sub>) corrosion. Moreover, in most cases, the formation of iron sulfide layers plays a key role in governing H<sub>2</sub>S corrosion. The complex mechanism of iron sulfide formation makes it difficult to quantify the H<sub>2</sub>S corrosion rate.<sup>2-6</sup> Some critical studies of H<sub>2</sub>S corrosion are outlined below.

Morris, et al.,<sup>7</sup> used a mild steel rotating disc electrode (RDE) to study corrosion in aqueous solutions of acid pH (pH 3 to pH 4) with H<sub>2</sub>S. They found that the presence of H<sub>2</sub>S shifted the anodic polarization curves of steel toward more negative potentials in weak acid solutions, with Tafel slopes of the anodic processes at ~0.041 V/decade. They also found that a cathodic limiting current density in an acidic solution gradually disappeared as the concentration of H<sub>2</sub>S increased. They concluded the process was under activation control and the Tafel slope did not change with H<sub>2</sub>S, staying consistently in the range

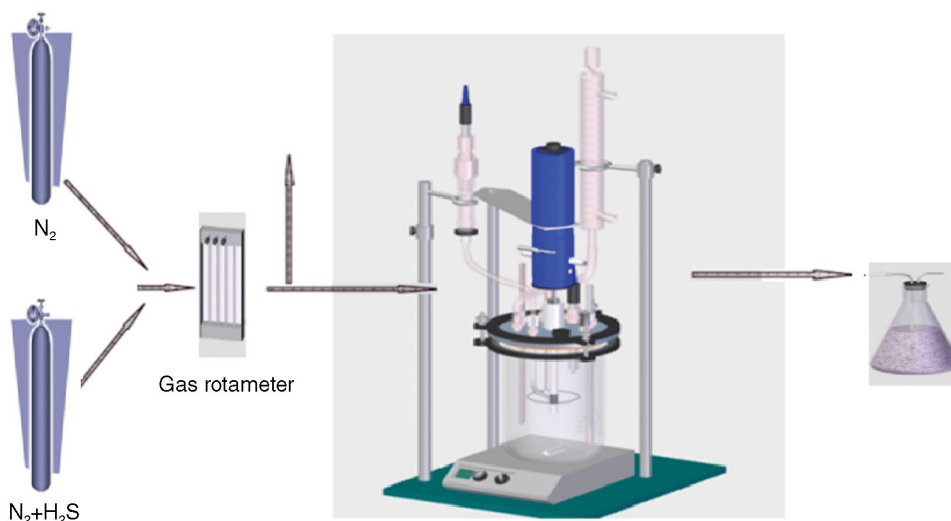


FIGURE 1. Schematic of the experimental cell.

from  $b_c = 0.110$  V/decade to  $0.116$  V/decade. They found the corrosion reaction order with  $H_2S$  to be  $n_{H_2S} = (\partial \log i_{corr} / \partial \log [H_2S]) = 0.2$ . Iofa, et al.,<sup>8</sup> also found acceleration effects of  $H_2S$  on the anodic reaction and attributed this effect to the chemisorptions and catalysis of  $H_2S$ . Shoosmith, et al.,<sup>2</sup> proposed a similar anodic reaction mechanism to Iofa's and suggested a solid-state reaction for iron sulfide formation. Cheng, et al.,<sup>9</sup> found the anodic dissolution current ( $i_a$ ) increased with pH and  $H_2S$  concentration with reaction orders of about  $n_{pH} = n_{H_2S} = 0.25$ , and  $i_{corr}$  increased with  $[H_2S]$  by a reaction order  $n_{H_2S} = [\partial \log i_{corr} / \partial \log [H_2S]]_{pH,E} = 0.20$  when  $[H_2S]/[H_3O^+] < 10^{1.5}$ . Recently, Sun and Nešić<sup>10</sup> proposed a mechanistic model based on a mass-transfer control mechanism for corrosion in the presence of protective iron sulfide layers, often seen in  $H_2S$  corrosion.

Despite many studies that have appeared in the literature, many questions still need to be answered regarding the effect of  $H_2S$  on mild steel corrosion. Some of the key ones are:

- Is there an additional cathodic reaction—direct  $H_2S$  reduction? Direct  $H_2S$  reduction has been proposed by several authors, but direct evidence for its existence is still not available.
- How does the  $H_2S$  affect the anodic reaction of iron dissolution?
- What is the mechanism and kinetics of formation and growth of an FeS layer?
- How does an FeS layer affect the cathodic reactions and the anodic reaction?

The objective of the present work was to seek answers to the first two questions. Therefore, an experimental study was organized where corrosion of mild steel was examined by electrochemical techniques, in short-term experiments (before any FeS layers formed), in solutions at various pH and different temperatures, under various  $H_2S/N_2$  gas concentration

ratios and flow rate conditions, using an X65 mild steel rotating cylinder electrode. The third question was previously addressed by the work of Sun and Nešić<sup>10</sup> and is currently being scrutinized. The last question will be addressed in future work.

## EXPERIMENTAL PROCEDURES

### Equipment

Experiments were conducted at atmospheric pressure in a 2 L glass cell (Figure 1) with a 1 wt% sodium chloride (NaCl) in deionized water solution. Gas (mixture of  $H_2S$  and  $N_2$ ) was purged through the cell continuously. A three-electrode setup was used. A rotating cylinder electrode (RCE) with a speed control unit was used as the working electrode (WE). A platinum wire was used as a counter electrode (CE). A saturated silver/silver chloride (Ag/AgCl) reference electrode (RE) was connected to the cell externally via a Luggin capillary. The pH was monitored with an electrode immersed in the electrolyte. The gaseous concentration of  $H_2S$  was adjusted by using a gas rotameter and confirmed by using a gas sample pump with  $H_2S$  detector tubes. A carbon scrubber was used to treat the gas coming out of the glass cell to remove the  $H_2S$ .

### Material

Corrosion of X65 pipeline steel was investigated. The composition of the X65 steel (as reported by the manufacturer) used in the present experiments is shown in Table 1. The WE was machined from the parent steel material and had a diameter of 1.20 cm and a working surface area of  $5.4 \text{ cm}^2$ .

### Procedure

The aqueous solution was initially purged with  $N_2$  gas for at least three hours to remove traces of dis-

**TABLE 1**  
Chemical Composition of 5L X65 Used in Rotating Cylinder Electrode (wt%)

Cr	Mo	S	V	Si	C	Fe	Ni	Mn	P
0.14	0.16	0.009	0.047	0.26	0.13	Balance	0.36	1.16	0.009

solved oxygen. After the solution was deoxygenated, H<sub>2</sub>S was dissolved by purging for at least half an hour to saturate the solution at the required partial pressure of H<sub>2</sub>S. H<sub>2</sub>S gas concentration was adjusted by purging different ratios of N<sub>2</sub> and H<sub>2</sub>S gas, from 100 ppm(v) to 10%(v) H<sub>2</sub>S (g) (g stands for gas phase, otherwise H<sub>2</sub>S is always referring to the aqueous H<sub>2</sub>S phase if not particularly indicated), corresponding to a H<sub>2</sub>S(g) partial pressure p<sub>H<sub>2</sub>S</sub> = 0.1 mbar and 96.5 mbar, respectively, at 30°C. The pH was adjusted by adding a deoxygenated hydrochloric acid (HCl) or sodium hydroxide (NaOH). Prior to immersion, the mild steel specimen surfaces were polished with 400 grit and 600 grit sandpaper, rinsed with alcohol, and dried with an air blower.

Polarization resistance (R<sub>p</sub>) measurements were conducted by polarizing the WE ±5 mV from the open-circuit potential (OCP) and scanning at 0.125 mV/s. Solution resistance was measured independently using electrochemical impedance spectroscopy (EIS), and the measured R<sub>p</sub> then was corrected. The linear polarization resistance (LPR) constant, B = 23 mV/decade, used in this work was determined from longer term weight-loss measurements. EIS measurements were carried out by applying an oscillating potential ±5 mV around the free corrosion potential of the WE, using the frequency range 3 mHz to 5 kHz. At the end of each experiment, the potentiodynamic sweeps were conducted at a sweep rate of 1 mV/s. The cathodic sweep was performed first by commencing at the OCP; then the electrode was allowed to equilibrate back to the OCP, and finally the anodic sweep starting at the OCP was performed. The solution resistance was manually corrected after the measurements. The test matrix for the experimental work is shown in Table 2.

## RESULTS AND DISCUSSION

### Effect of p<sub>H<sub>2</sub>S</sub>

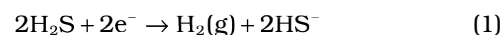
Effects of H<sub>2</sub>S on polarization curves at different pH and 1,000 rpm rotating speed conditions are shown in Figures 2 through 4. At pH 4, the cathodic polarization curve for a pure N<sub>2</sub> environment (without any H<sub>2</sub>S) shows the typical characteristics, consisting of H<sup>+</sup> (proton) reduction and H<sub>2</sub>O (water) reduction. A mass-transfer-limiting current plateau is observed. The Tafel slope of H<sub>2</sub>O reduction is close to 120 mV/decade. The addition of 100 ppm(v) or 1,000 ppm(v) H<sub>2</sub>S(g) does not change the cathodic polarization curves much, but it results in a lower H<sub>2</sub>O reduction rate, which indicates a retardation effect possibly due

**TABLE 2**  
Experimental Conditions

Description	Parameters
Test material	API 5L X65
Test solution	1 wt% NaCl solution
Purged gas (H <sub>2</sub> S gas volume fraction in H <sub>2</sub> S/N <sub>2</sub> )	0 to 10%(v) (0 to 0.1 bar)
Rotating speed/rpm	200 to 4,000 rpm
Total pressure/bar	1
Temperature/°C	30°C, 60°C, 80°C
pH	2 to 5
Test duration	0.5 to 2
Measurement methods	LPR, EIS, potentiodynamic sweeps, weight loss

to surface coverage by a sulfide species. The H<sub>2</sub>O reduction rate in an H<sub>2</sub>S-saturated aqueous environment is found to be approximately 20 times lower than in the same solution without H<sub>2</sub>S. This retardation effect of H<sub>2</sub>O reduction is observed at all experimental conditions with H<sub>2</sub>S, even at a lower pH levels, i.e., pH 2, where iron sulfide should not be able to form. Therefore, the retardation effect of the H<sub>2</sub>O reduction reaction is not considered to be related to iron sulfide formation.

At the same pH 4, when 1%(v) or 10%(v) H<sub>2</sub>S(g) was introduced, the cathodic polarization curves show a higher limiting current (plateau) at more cathodic potentials, often referred to as “the second wave.” It is hypothesized here that this is an indication of the direct reduction of H<sub>2</sub>S on the steel surface according to:



Tests conducted at a higher pH 5 were able to better distinguish this direct H<sub>2</sub>S reduction from H<sup>+</sup> reduction. From Figure 3, at pH 5 in a N<sub>2</sub> environment (no H<sub>2</sub>S), the cathodic contribution from H<sup>+</sup> reduction becomes smaller and the direct H<sub>2</sub>O reduction is the dominant cathodic reaction. The cathodic polarization curve appears almost as a straight line; no mass-transfer-limiting current plateau is observed. With 100 ppm(v) H<sub>2</sub>S(g), the additional contribution from H<sub>2</sub>S is still not clearly seen. However, in the presence of 10%(v) H<sub>2</sub>S(g), the contribution of H<sub>2</sub>S reduction to the total corrosion current becomes dominant. The existence of an additional electrochemical reaction—direct H<sub>2</sub>S reduction seems to be clear.

The effect of H<sub>2</sub>S on the anodic iron dissolution reaction can also be seen in these polarization curves.

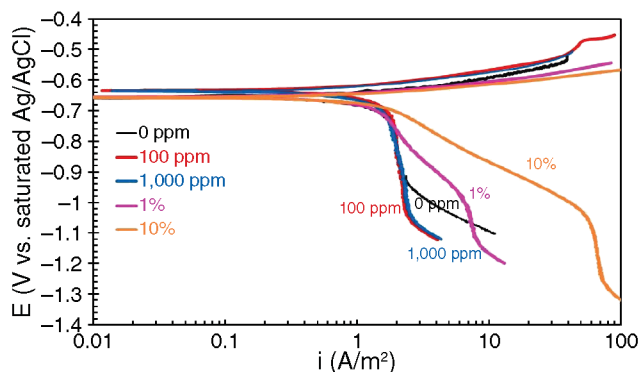


**FIGURE 2.** Effect of  $H_2S$  on polarization curves at pH 4, 30°C, total pressure 1 bar, 1 wt% NaCl, 1,000 rpm.

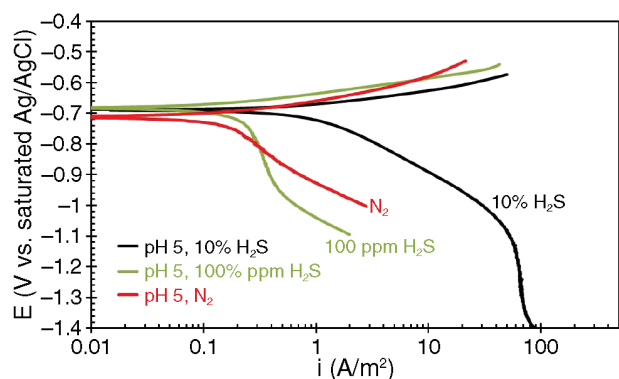


**FIGURE 3.** Effect of  $H_2S$  on polarization curves at pH 5, 30°C, total pressure 1 bar, 1 wt% NaCl, 1,000 rpm.

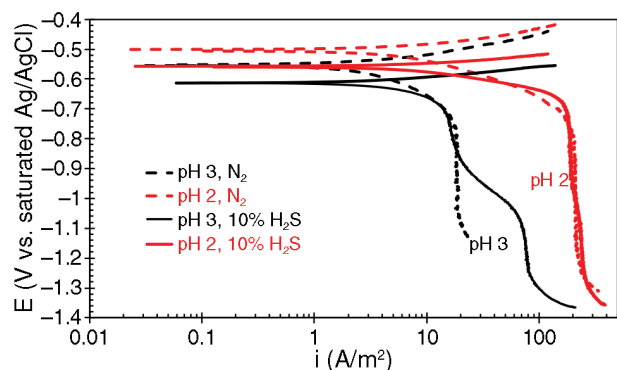


**FIGURE 4.** Effect of  $H_2S$  on polarization curves at pH 3 and pH 2, 30°C, total pressure 1 bar, 1 wt% NaCl, 1,000 rpm.

At pH 4 (Figure 2), with 100 ppm(v) and 1,000 ppm(v)  $H_2S$ (g), the anodic polarization curves shift to the left as compared with the one in the  $N_2$  environment, which indicates a retardation effect due to  $H_2S$ . With 1%(v) and 10%(v)  $H_2S$ (g), the anodic polarization curve shifts to the right, suggesting an accelerating effect due to  $H_2S$ . This accelerating effect of  $H_2S$  on the anodic reaction of iron dissolution can be observed more clearly from the anodic polarization curves obtained at more acid conditions, pH 2 and pH 3 (Figure 4). This

observation also agrees with the previous researchers.<sup>7-9</sup> The accelerating effect seems to be related to sulfide adsorption.

From the results discussed above, it can be summarized that the presence of  $H_2S$  affects both anodic reaction and cathodic reaction. There is a complex effect of  $H_2S$  on the anodic dissolution of iron and an appearance of a new additional cathodic reaction: direct  $H_2S$  reduction.

### Effect of Flow/Mass-Transfer Rate

To further elucidate the electrochemical corrosion mechanisms in the presence of  $H_2S$ , mass-transfer conditions were altered by changing the turbulent flow conditions. The effect of flow/mass-transfer rate on the polarization curves for the 1%(v)  $H_2S$ (g) condition is shown in Figure 5. At this condition, the dominant cathodic reactions are  $H^+$  reduction, direct  $H_2S$  reduction, and  $H_2O$  reduction. The mass-transfer limitation for  $H^+$  and  $H_2S$  reduction gives rise to two “waves” in the cathodic curve, denoting two limiting current plateaus. Water reduction is under charge-transfer control, which is flow/mass-transfer-independent. The reduction rates of  $H^+$  and  $H_2S$  are influenced by the diffusion of reactants to the surface, so that, at a given flow rate, the total mass-transfer-limiting current,  $i_{lim}$ , for mild steel in an  $H_2S$ -saturated solution can be described by the additive contribution of two components:

$$i_{lim} = i_{lim,H^+} + i_{lim,H_2S} \quad (2)$$

where  $i_{lim,H^+}$  and  $i_{lim,H_2S}$  are the limiting current densities obtained in turbulent flow conditions for  $H^+$  ions and  $H_2S$  molecules, respectively. The limiting current density for the newly identified cathodic reaction— $H_2S$  reduction, which can be seen clearly in Figure 5, is found to be in good agreement with the theoretical mass-transport-limiting current calculated by using the Eisenberg expression,<sup>11</sup> which is shown in the model validation part.

From Figure 5, all the anodic curves displayed clear Tafel behavior, with a slope of  $\approx 40$  mV/decade to 50 mV/decade. No effect of rotating speed on the anodic reaction was noticed, as expected.

Polarization curves for the solution purged with 10%(v)  $H_2S$ (g) at pH 4 are shown in Figure 6. The overall shape of the curves was slightly different compared to those in the experiments with 1%(v)  $H_2S$ (g). The second “wave” on the cathodic polarization curves is not as clearly observed because it was at 1%(v)  $H_2S$ (g). This is because the bulk concentration of  $H_2S$  is 10 times higher than before, and thereby the limiting current “wave” from  $H_2S$  reduction is masking the much smaller limiting current “wave” from  $H^+$  reduction. Therefore, the mass-transfer-limiting current in this case is mostly attributed to the reduction of  $H_2S$ . The magnitude of the mass-transfer-limiting current

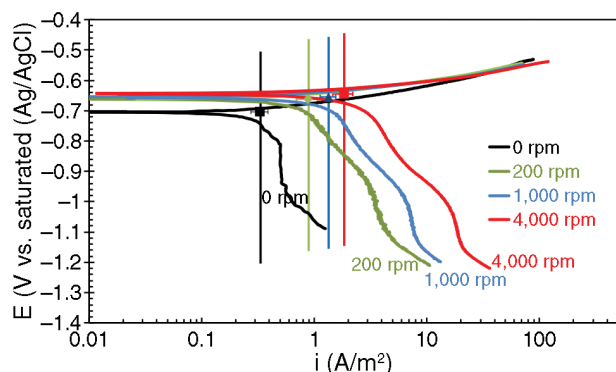


**FIGURE 5.** Effect of flow rate on polarization curves at 1%(v)  $H_2S(g)$ , pH 4, 30°C, total pressure 1 bar, 1 wt% NaCl. Vertical lines are corrosion currents measured by LPR using  $B = 23$  mV/decade.

density for the reduction of  $H_2S$  obtained in this test is also in good agreement with the prediction made by the Eisenberg expression,<sup>11</sup> which is shown in the model validation part.

Both the tests at 1%(v)  $H_2S(g)$  and 10%(v)  $H_2S(g)$  confirmed that the direct reduction of  $H_2S$  is flow-sensitive. The mass-transfer-limiting currents were observed and could be calculated by using mass-transfer correlations such as the correlation of Eisenberg, et al., for a rotating cylinder. Morris, et al., concluded that a limiting current density in an acidic solution gradually disappears as the concentration of  $H_2S$  increased.<sup>7</sup> But, from a review of their published data, it appears that they had not polarized the steel low enough (in the cathodic direction) to see the appearance of the mass-transfer-limiting current. The current work extends their results to show that the limiting current density does increase as the concentration of  $H_2S$  is increased.

Moreover, from Figures 5 and 6, it is seen that the corrosion currents,  $i_{corr}$ , measured by LPR (shown as vertical lines) are much smaller than the mass-transfer-limiting currents, which indicates that the  $H_2S$  corrosion is not always under mass-transfer control, as previously assumed by Sun and Nešić.<sup>10</sup>

### Effect of pH

**Solution Without  $H_2S$**  — The effect of pH in a solution without  $H_2S$  is shown in Figure 7. The  $i_{lim,H^+}$  values measured at 1,000 rpm scaled proportionately to the  $H^+$  concentration. The position/magnitude of the Tafel line for  $H_2O$  reduction stayed approximately the same over the whole pH range, with a slope of  $\approx 120$  mV/decade. This was in accordance with theory and agreed with the findings of Nešić, et al.<sup>12</sup>

The analysis of anodic polarization curves showed that the Tafel line for anodic dissolution of iron maintained the slope of 40 mV/decade to 50 mV/decade over the whole pH range tested. The increase of the anodic exchange current density was significant from pH 2 to pH 4 and much less between pH 4 and pH 5,

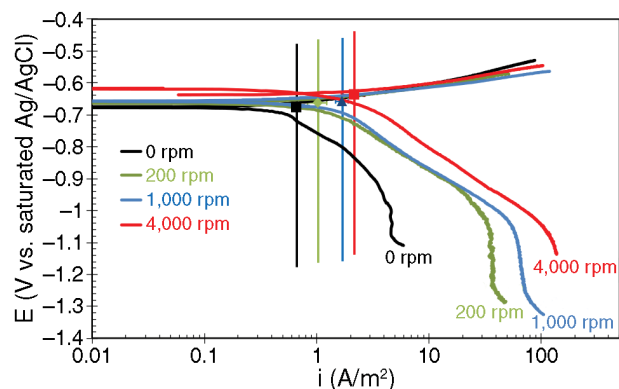


**FIGURE 6.** Effect of flow rate on polarization curves at 10%(v)  $H_2S(g)$ , pH 4, 30°C, total pressure 1 bar, 1 wt% NaCl. Vertical lines are representing the magnitude LPR corrosion currents derived from polarization resistance measurements by using  $B = 23$  mV/decade.

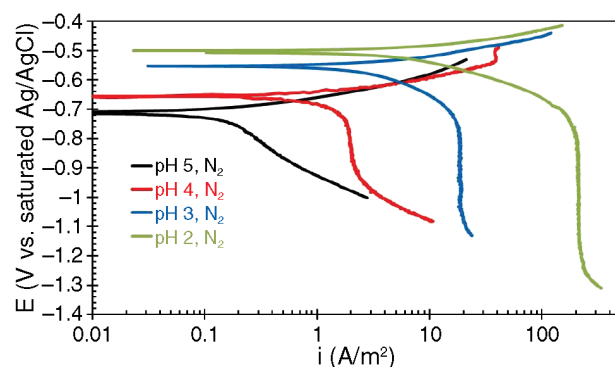


**FIGURE 7.** Effect of pH on polarization curves in the solution purged with  $N_2$ , 1,000 rpm, 30°C, total pressure 1 bar, 1 wt% NaCl.

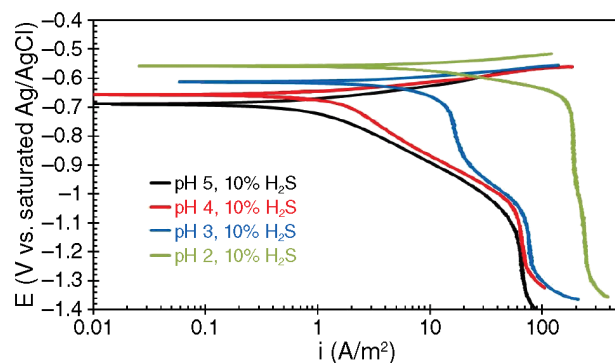


**FIGURE 8.** Effect of pH on polarization curves in the solution purged with 10%(v)  $H_2S(g)$ , 1,000 rpm, 30°C, total pressure 1 bar, 1 wt% NaCl.

which is in agreement with the findings of Bockris, et al.<sup>13</sup>

**Solution with  $H_2S$**  — The effect of pH in a solution saturated with 10%(v)  $H_2S(g)$  is shown in Figure 8. The decrease in limiting current is much less than expected from pH 3 to pH 5, accounting for a orders of magnitude change in  $H^+$  concentration. This suggests

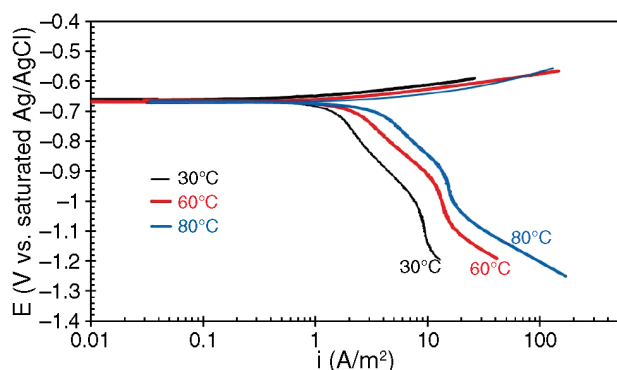


**FIGURE 9.** Polarization curves at pH 4 for temperatures 30°C, 60°C, and 80°C,  $[H_2S]_{aq} = 8.3 \times 10^{-4}$  mol/L, 1,000 rpm, total pressure 1 bar, 1 wt% NaCl.

that the cathodic reaction was not solely comprised of  $H^+$  reduction. The reason in this case is that the main contribution for the cathodic limiting current from pH 3 to pH 5 is from the  $H_2S$  species, whose concentration is independent of pH value. The exception is pH 2 where the main contribution for cathodic limiting current is from  $H^+$ , while only a small “bump” on the limiting current plateau can still be observed due to the additional  $H_2S$ .

From Figure 8 it can be seen that the  $H_2O$  reduction curve at 10%(v)  $H_2S(g)$  stayed approximately the same over the whole pH range, except at pH 5, which was most likely caused by an experimental error. Figure 8 also shows that pH had a smaller effect on the anodic dissolution reaction at 10%(v)  $H_2S(g)$ , especially from pH 3 to pH 5, which is different from the results obtained without  $H_2S$ . According to the finding of Cheng, et al.,<sup>9</sup> anodic dissolution current ( $i_a$ ) is independent of pH and  $pH_2S$  when  $[H_2S]/[H^+] > 10^{1.5}$ . As can be seen from the first dissociation of  $H_2S$  in solution:



$$K_{H_2S} = \frac{[H^+][HS^-]}{[H_2S]} \quad (4)$$

Actually, the ratio of  $[H_2S]_a/[H^+]$  is equal to  $[HS^-]/K_{H_2S}$ . Anodic dissolution current will reach a maximum value when  $HS^-$  exceeds a specific concentration at a specific temperature.

### Effect of Temperature

To investigate the effect of temperature in the presence of  $H_2S$ , experiments were conducted at the same aqueous  $H_2S$  concentration,  $[H_2S]$ , using different gas concentrations of  $H_2S$  at each temperature (30°C, 60°C, and 80°C) to maintain an approximate  $[H_2S] = 8.3 \times 10^{-4}$  mol/L.

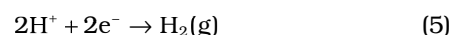
Corrosion rate measured from LPR increased from 1.6 mm/year at 30°C to 5.0 mm/year at 80°C.

This change of corrosion rate can be explained from the polarization curves obtained at different temperatures as shown in Figure 9. Temperature is known to accelerate most of the chemical, electrochemical, and transport processes occurring in the system, and both cathodic reactions and anodic currents, which were measured, increased with increasing temperature. The increase of anodic current is not as significant as the one stemming from cathodic reactions. Water reduction current and the limiting current also increase with increasing temperature.

## PHYSICO-CHEMICAL MODEL

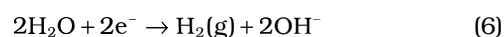
### Cathodic Reactions

When  $H_2S$  is not present in the water, the main cathodic reaction is hydrogen evolution via the reduction of free  $H^+$  ions:



which is the most important cathodic reaction in an acidic solution ( $pH < 4$ ). In the case of mild steel corrosion, this reaction is usually limited by the rate at which  $H^+$  ions are transported from the bulk solution to the steel surface (mass-transfer limitation).

As the availability of  $H^+$  ions decreases, in more neutral solutions ( $pH > 5$ ), hydrogen evolution via the direct reduction of water may become important:



When  $H_2S$  is present in the water, the following additional reactions occur:

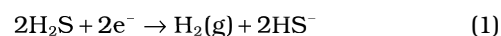
— $H_2S$  gas dissolves in water to form aqueous  $H_2S$ :



—Aqueous  $H_2S$  is a mild acid that partly dissociates in two steps:



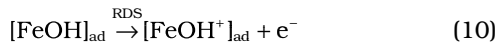
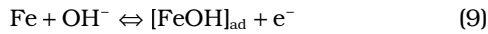
to provide additional  $H^+$  ions. However, as it has been experimentally proven in this work, adsorbed  $H_2S$  can also be an electron acceptor,<sup>14</sup> and the evolution of hydrogen can occur via the so-called direct reduction of  $H_2S$ :



This reaction has a limiting current that is controlled by a mass-transfer rate of  $H_2S$  from bulk solution to the steel surface, and is therefore sensitive to flow.

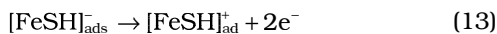
### Anodic Reaction

Bockris, et al.,<sup>13</sup> proposed the following mechanism of anodic iron dissolution in strong acids (pH ≤ 4), which applies here to cases when H<sub>2</sub>S was not present in the system:

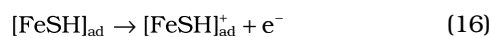
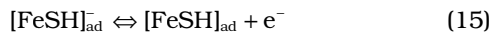


This mechanism suggests that the reaction order with respect to OH<sup>-</sup> ions is 1, which is proven to be valid in acidic solutions; it has also been found that iron dissolution proceeds with little influence of pH for solutions where pH is above approximately pH 4.<sup>13</sup>

In the presence of H<sub>2</sub>S, Shoesmith, et al.,<sup>2</sup> proposed:



In this mechanism, two electrons are released in one step, which is not likely. However, the iron dissolution mechanism can be rewritten to appear similar to the one proposed by Bockris, et al., this time for solution containing H<sub>2</sub>S, as proposed by Ma, et al.:<sup>15</sup>



### MATHEMATICAL MODEL

To describe mathematically and numerically the physicochemical model, the measured cathodic and anodic currents reported above are used as a basis.

#### H<sup>+</sup> Reduction

For H<sup>+</sup> reduction, to describe the effect of charge transfer and mass transfer on H<sup>+</sup> reduction, the current density for reduction of H<sup>+</sup> can be thought of as consisting of two components: charge-transfer current and mass-transfer-limiting current. Total current density is calculated using a harmonic mean:<sup>12</sup>

$$\frac{1}{i_{\text{H}^+}} = \frac{1}{i_{\alpha, \text{H}^+}} + \frac{1}{i_{\text{lim}, \text{H}^+}^{\text{d}}} \quad (17)$$

where  $i_{\text{H}^+}$  is total current density of H<sup>+</sup> reduction (A/m<sup>2</sup>),  $i_{\alpha, \text{H}^+}$  is the charge-transfer current density (A/m<sup>2</sup>), and  $i_{\text{lim}, \text{H}^+}^{\text{d}}$  is the diffusion-limiting current density.

The charge-transfer current density can be calculated using the Tafel equation as:

$$i_{\alpha, \text{H}^+} = i_{0, \text{H}^+} \times 10^{\frac{\eta}{b_c}} \quad (18)$$

where  $i_{0, \text{H}^+}$  is the exchange current density (A/m<sup>2</sup>),  $b_c$  is the cathodic Tafel slope (V/decade), and  $\eta$  is the over potential (V), which is equal to the difference between the operating (actual) potential and the reversible potential.

The cathodic Tafel slope,  $b_c$ , can be calculated from:

$$b_c = \frac{2.303RT}{\alpha_c F} \quad (19)$$

According to Bockris, et al.,<sup>13</sup> for H<sup>+</sup> reduction,  $\alpha_c = 0.5$ , giving  $b_c \approx 0.120$  V/decade at 30°C. This agreed well with the present findings.

The reversible potential of hydrogen reduction can be calculated as:

$$E_{\text{rev}(\text{H}^+)} = -\frac{2.303RT}{F} \text{pH} - \frac{2.303RT}{2F} \log P_{\text{H}_2} \quad (20)$$

where the partial pressure of hydrogen normally is assumed to be close to zero. The only unknown model parameter for calculating the charge-transfer current density is the exchange current density,  $i_{0, \text{H}^+}$ . According to Nordsveen, et al.,<sup>16</sup>  $i_{0, \text{H}^+}$  can be calculated by:

$$i_{0, \text{H}^+} = i_0^{\text{ref}} \left( \frac{C_{\text{H}^+}}{C_{\text{H}^+}^{\text{ref}}} \right)^{0.5} \times e^{\frac{\Delta H}{R} \left( \frac{1}{T} - \frac{1}{T_{\text{ref}}} \right)} \quad (21)$$

where  $i_0^{\text{ref}}$  is the reference exchange current density at a reference temperature,  $T_{\text{ref}}$  (K), and reference concentration of H<sup>+</sup>.  $\Delta H$  is the enthalpy of activation for the H<sup>+</sup> reduction reaction (J/mol).

The  $i_0^{\text{ref}}$  for H<sup>+</sup> reduction was taken as 0.03 A/m<sup>2</sup> at reference temperature 20°C and reference H<sup>+</sup> concentration 1×10<sup>-4</sup> mol/L. The enthalpy of activation was taken as 30 kJ/mol.<sup>16</sup> No effect of H<sub>2</sub>S on H<sup>+</sup> reduction was found in our experiments.

**Limiting Current for H<sup>+</sup> Reduction** — The diffusion-limiting current appearing in Equation (17) is calculated with:

$$i_{\text{lim}, \text{H}^+}^{\text{d}} = k_{\text{m}, \text{H}^+} F C_{\text{H}^+} \quad (22)$$

where  $k_{\text{m}, \text{H}^+}$  is H<sup>+</sup> mass-transfer coefficient (m/s) and  $C_{\text{H}^+}$  is the bulk concentration of H<sup>+</sup> (mol/m<sup>3</sup>).

Mass-transfer coefficient of H<sup>+</sup> can be calculated from a rotating cylinder correlation by Eisenberg, et al.<sup>11</sup>

$$\text{Sh} = \frac{k_{\text{m}, \text{H}^+} d_{\text{RCE}}}{D_{\text{H}^+}} = 0.0791 \times \text{Re}^{0.7} \times \text{Sc}^{0.356} \quad (23)$$

where  $Sh$  is the Sherwood number,  $d_{RCE}$  is the pipe diameter (m),  $D_{H^+}$  is the diffusion coefficient of hydrogen ion ( $m^2/s$ ),  $Re$  is Reynolds number =  $\rho u d_{RCE}/\mu$ , and  $Sc$  is the Schmidt number =  $\mu/\rho D_{H^+}$ .

In a dilute solution, the diffusion coefficient of species can be calculated using the Stokes-Einstein equation:

$$D_{H^+} = D_{ref(H^+)} \times \frac{T_k}{T_{ref}} \times \frac{\mu_{ref}}{\mu} \quad (24)$$

where  $D_{ref}$  is the reference diffusion coefficient at a reference temperature,  $\mu$  is the water viscosity in  $kg/m\cdot s$ , and  $\mu_{ref}$  is the reference viscosity at a reference temperature.  $D_{ref(H^+)}$  was taken as  $9.31 \times 10^{-9} m^2/s^{17}$  and  $\mu_{ref}$  was taken as  $1.002 kg/(m\cdot s)^{18}$  at reference temperature (293.15 K).

The temperature dependence of water density and water viscosity can be given as:

$$\rho = 1152.3 - 0.5116 \times T_k \quad (25)$$

$$\mu = \mu_{ref} \times 10^{\frac{1.3272(20 - T_c) - 0.001053(20 - T_c)^2}{T_c + 105}} \quad (26)$$

where  $T_c$  and  $T_k$  are temperature in  $^{\circ}C$  and Kelvin, respectively.

### Direct $H_2S$ Reduction

$H_2S$  takes part in the corrosion process in two main ways. First, by dissociation, it can provide an additional source of  $H^+$  which can be reduced. Second,  $H_2S$  can be directly reduced on the steel surface and further increase the corrosion rate.

It has been shown that the current density for the direct reduction of  $H_2S$  could be limited either by charge transfer or mass transfer. The total current density is given by:

$$\frac{1}{i_{H_2S}} = \frac{1}{i_{\alpha, H_2S}} + \frac{1}{i_{lim, H_2S}^d} \quad (27)$$

where  $i_{H_2S}$ ,  $i_{\alpha, H_2S}$ , and  $i_{lim, H_2S}^d$  are total current density, charge-transfer current density, and mass-transfer-limiting current density of this reaction in  $A/m^2$ , respectively.

Charge-transfer current density of this reaction can be calculated using the equation:

$$i_{\alpha, H_2S} = i_{0, H_2S} \times 10^{\frac{\eta}{b_c}} \quad (28)$$

where  $i_{0, H_2S}$  is the exchange current density ( $A/m^2$ ),  $b_c$  is the cathodic Tafel slope (V/decade) for  $H_2S$  reduction, and  $\eta$  is the over potential (V), which is equal to the difference between the operating (actual) potential and the reversible potential.

*Tafel Slope* — From the experiments, the cathodic Tafel slope,  $b_c$ , for  $H_2S$  reduction in Equation (24) was found to be close to 120 mV/decade at  $30^{\circ}C$ , which is the same as the value used for  $H^+$  reduction. The value of  $b_c$  can be calculated from Equation (19).

*Exchange Current Density* — From the best fit to experimental results at different concentrations of  $H_2S$  at pH 4, the order  $n$  of the reaction with respect to  $C_{H_2S}$  is found to be:

$$\frac{\partial \log i_{0, H_2S}}{\partial \log C_{H_2S}} \approx 0.5 \quad (29)$$

The same reaction order of 0.5 was also suggested by Kittel, et al.<sup>19</sup> It is similar to the one associated with the exchange current density of  $H^+$  reduction. Morris, et al.,<sup>7</sup> and Cheng, et al.,<sup>9</sup> stated the corrosion reaction order with  $H_2S$ :  $n = (\log i_{corr}/\log[H_2S]) = 0.2$ . However,  $i_{corr}$  includes both contributions from  $H^+$  and  $H_2S$  reduction. Under their experimental conditions (pH from 0.75 to 4), the contribution from  $H^+$  is dominant and would not allow an accurate calculation of the  $H_2S$  reduction reaction order.

Therefore, the exchange current density can be calculated as:

$$i_{0, H_2S} = i_{0, H_2S}^{ref} \left( \frac{C_{H_2S}}{C_{H_2S}^{ref}} \right)^{0.5} \left( \frac{C_{H^+}}{C_{H^+}^{ref}} \right)^{-0.5} \times e^{\frac{\Delta H}{R} \left( \frac{1}{T} - \frac{1}{T_{ref}} \right)} \quad (30)$$

where the  $i_{0, H_2S}^{ref}$  for  $H_2S$  reduction is  $0.00015 A/m^2$  at reference temperature 293.15 K and reference  $H^+$  concentration,  $1 \times 10^{-4} mol/L$ , and reference  $H_2S$  concentration,  $1 \times 10^{-4} mol/L$ . This means that the  $H_2S$  reduction rate is about 200 times slower than the  $H^+$  reduction rate ( $0.03 A/m^2$ ) at the same condition. The enthalpy of activation was taken as 60 kJ/mol from the best fit to experimental results.

*Reversible Potential* — The two electrochemical reactions—the reduction of  $H_2S$  and  $H^+$ —are equivalent thermodynamically and have the same reversible potential given by Equation (20).

*Limiting Current Density* — Calculation of limiting current density for  $H_2S$  reduction is similar to that for  $H^+$  reduction. The mass-transfer-limiting current density of this reaction is given by:

$$i_{lim, H_2S}^d = k_{m, H_2S} F C_{H_2S} \quad (31)$$

$$Sh = \frac{k_{m, H_2S} d_{RCE}}{D_{H_2S}} = 0.0791 \times Re^{0.7} \times Sc^{0.356} \quad (32)$$

$$D_{H_2S} = D_{ref(H_2S)} \times \frac{T_k}{T_{ref}} \times \frac{\mu_{ref}}{\mu} \quad (33)$$

where  $D_{ref(H_2S)}$  was taken as  $1.61 \times 10^{-9} m^2/s$  at reference temperature (293.15 K).<sup>20</sup> The concentration of  $H_2S$  can be calculated by:

$$C_{\text{H}_2\text{S}} = K_{\text{sol}(\text{H}_2\text{S})} \times p_{\text{H}_2\text{S}} \quad (34)$$

where  $p_{\text{H}_2\text{S}}$  is partial pressure of  $\text{H}_2\text{S}$  in bar, and  $K_{\text{sol}(\text{H}_2\text{S})}$  is Henry's constant in mol/bar, which is given by Equation (35):<sup>21</sup>

$$K_{\text{sol}(\text{H}_2\text{S})} = 10^{-\left(634.27 + 0.2709T_k - 0.11132 \times 10^{-3}T_k^2 \frac{16719}{T_k} - 261.9 \log T_k\right)} \quad (35)$$

### Water Reduction

Since water molecules are present in unrestricted quantities at the metal surface, it can be assumed that at all times the reduction rate of  $\text{H}_2\text{O}$  is controlled by the charge-transfer process and, hence, the Tafel equation is used:

$$i_{\text{H}_2\text{O}} = i_{0,\text{H}_2\text{O}} \times 10^{-\frac{\eta}{b_c}} \quad (36)$$

Tafel slope for this reaction in all experiments at 30°C was found to be close to 120 mV/decade, which is the same as that for  $\text{H}^+$  reduction. Tafel slope for  $\text{H}_2\text{O}$  reduction is given by Equation (19).

Since the electrochemical reduction of  $\text{H}_2\text{O}$  and  $\text{H}^+$  are equivalent thermodynamically, the reversible potential and  $\text{H}_2\text{O}$  reduction were assumed to be the same as for  $\text{H}^+$  reduction, which is calculated by Equation (20).

*Exchange Current Density* — When  $\text{H}_2\text{S}$  is not present, the exchange current density for  $\text{H}_2\text{O}$  reduction is given by:

$$i_{0,\text{H}_2\text{O}} = i_0^{\text{ref}} \left( \frac{C_{\text{H}^+}}{C_{\text{H}^+\text{ref}}} \right)^{-0.5} e^{\frac{\Delta H}{R} \left( \frac{1}{T} - \frac{1}{T_{\text{ref}}} \right)} \quad (37)$$

The  $i_{0,\text{ref}}$  for  $\text{H}_2\text{O}$  reduction was  $2 \times 10^{-5} \text{ A/m}^2$  at reference temperature 293.15 K and reference  $\text{H}^+$  concentration  $1 \times 10^{-4} \text{ mol/L}$ . The enthalpy of activation was taken as 30 kJ/mol.<sup>12</sup>

When  $\text{H}_2\text{S}$  is present, apparently it can retard the  $\text{H}_2\text{O}$  reduction, resulting in rates about 20 times lower than that seen in environments without  $\text{H}_2\text{S}$ . From the current experimental results, the reaction order  $\log i_{0,\text{H}_2\text{O}}/\log[\text{H}_2\text{S}]$  is close to 0.1. The exchange current density is given by:

$$i_{0,\text{H}_2\text{O}} = i_0^{\text{ref}} \left( \frac{C_{\text{H}^+}}{C_{\text{H}^+\text{ref}}} \right)^{-0.5} \left( \frac{C_{\text{H}_2\text{S}}}{C_{\text{H}_2\text{Sref}}} \right)^{-0.1} e^{\frac{\Delta H}{R} \left( \frac{1}{T} - \frac{1}{T_{\text{ref}}} \right)} \quad (38)$$

In an  $\text{H}_2\text{S}$  environment, the  $i_0^{\text{ref}}$  for  $\text{H}_2\text{O}$  reduction was  $1 \times 10^{-6} \text{ A/m}^2$  at reference temperature 293.15 K, the reference  $\text{H}^+$  concentration of  $1 \times 10^{-4} \text{ mol/L}$ , and the reference  $\text{H}_2\text{S}$  concentration of  $1 \times 10^{-4} \text{ mol/L}$ . The enthalpy of activation was 90 kJ/mol from the best fit to experimental results, which would suggest that  $\text{H}_2\text{O}$  reduction in an  $\text{H}_2\text{S}$  environment is more sensitive to temperature.

### Anodic Dissolution of Iron

In the present experiments, the anodic dissolution of iron was under charge-transfer control. Therefore, pure Tafel behavior can be assumed close to the corrosion potential:

$$i_{\text{Fe}} = i_{0,\text{Fe}} \times 10^{\frac{\eta}{b_a}} \quad (39)$$

The Tafel slopes of anodic reaction in  $\text{H}_2\text{S}$  environments or environments without  $\text{H}_2\text{S}$  are all close in the range from 40 mV/decade to 50 mV/decade. The introduction of  $\text{H}_2\text{S}$  did not have any effect on the Tafel slope, so for anodic iron dissolution, Tafel slope is given as:

$$b_a = \frac{2.303RT}{\alpha_a F} \quad (40)$$

According to Bockris, et al.,<sup>13</sup> the apparent symmetry coefficient for the anodic reaction of Fe dissolution was taken as 1.5, giving  $b_a = 40 \text{ mV}$  at 30°C, which is close to our experimental results. The reversible potential of X65 steel was taken<sup>12</sup> to be  $-0.488 \text{ V}$ .

*Exchange Current Density* — When  $\text{H}_2\text{S}$  is not present, according to the mechanism proposed by Bockris, et al.,<sup>13</sup> the reaction order with respect to  $\text{OH}^-$  ions is 1, which is valid in acidic solutions; it has been found that iron dissolution proceeds with little influence of pH for solutions above approximately pH 4. It is assumed that the exchange current density is proportional to the surface coverage of  $\text{OH}^-$  ( $\theta_{\text{OH}^-}$ ) and that it follows the Frumkin adsorption model:

$$i_{0,\text{Fe}} = i_{0,\text{Fe}}^* \theta_{\text{OH}^-} e^{\frac{\Delta H}{R} \left( \frac{1}{T} - \frac{1}{T_{\text{ref}}} \right)} \quad (41)$$

$$K_1 C_{\text{OH}^-} = \frac{\theta_{\text{OH}^-}}{1 - \theta_{\text{OH}^-}} e^{(-f\theta_{\text{OH}^-})} \quad (42)$$

According to the current experimental results and Bockris, et al.,<sup>13</sup> the best-fit values in Equations (41) and (42) are  $i_{0,\text{Fe}}^* = 0.25$ ,  $K_1 = 1.56 \times 10^9$ , and  $f = 3.83$ . Actually, when  $f$  is equal to 0, the Frumkin adsorption model becomes the Langmuir adsorption model. The reference temperature is 293.15 K. The activation energy,  $\Delta H$ , was set to be 37.5 kJ/mol, which is taken from the finding of Nordsveen, et al.<sup>16</sup>

The concentration of  $\text{OH}^-$  can be calculated by:

$$C_{\text{OH}^-} = \frac{K_{\text{wa}}}{C_{\text{H}^+}} \quad (43)$$

$K_{\text{wa}}$  is the equilibrium constant of the water dissociation reaction, which can be calculated by:<sup>22</sup>

$$K_{\text{wa}} = 10^{-\left(29.3868 - 0.0737549 \times T_k + 7.47881 \times 10^{-5} \times T_k^2\right)} \quad (44)$$

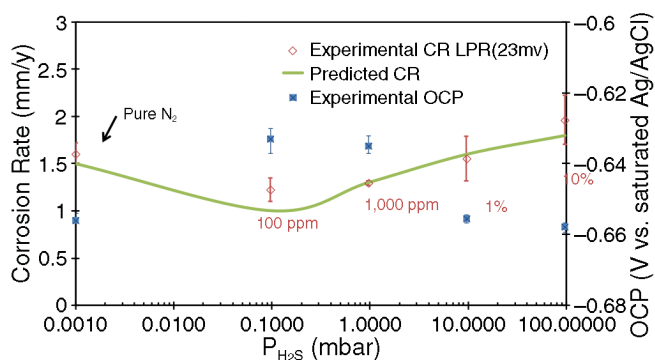


**FIGURE 10.** Comparison of corrosion rate predictions with LPR experimental results and experimental OCP at pH 4 and different  $H_2S$  concentrations, total pressure = 1.0 bar, 1,000 rpm 30°C,  $B = 23$  mV/decade.

When  $H_2S$  is present, according to the mechanism proposed previously, Equations (14), (15), and (16), the exchange current density for iron dissolution is related to  $HS^-$  concentration. Even at low concentrations of  $H_2S$ , such as 100 ppm(v)  $H_2S$  (0.1 mbar) and pH 4, the concentration of  $HS^-$  is much higher ( $1 \times 10^{-8}$  mol/L) than the concentration of  $OH^-$  ( $1 \times 10^{-10}$  mol/L). Therefore, the contribution of  $OH^-$  to the anodic reaction kinetics was ignored. It can be assumed that the exchange current density is only related to the surface coverage of  $HS^-$  ( $\theta_{HS^-}$ ) and that it follows the Langmuir adsorption model:

$$i_{0,Fe} = i_{0,Fe}^* \theta_{HS^-} e^{-\frac{\Delta H}{R} \left( \frac{1}{T} - \frac{1}{T_{ref}} \right)} \quad (45)$$

$$\theta_{HS^-} = \frac{K_2 C_{HS^-}}{1 + K_2 C_{HS^-}} \quad (46)$$

The best-fit values in Equations (45) and (46) for  $i_{0,Fe}^* = 0.33$ ,  $K_2 = 3.5 \times 10^6$ . The reference temperature is 293.15 K. The activation energy,  $\Delta H$ , was assumed to be the same as for an environment without  $H_2S$  (37.5 kJ/mol).  $C_{HS^-}$  is the concentration of  $HS^-$ , which is given by:

$$C_{HS^-} = \frac{K_{H_2S} C_{H_2S}}{C_{H^+}} \quad (47)$$

$K_{H_2S}$  is the equilibrium constant for the first dissociation of  $H_2S$ , which can be calculated by:<sup>23</sup>

$$K_{H_2S} = 10^{782.43945 + 0.361261 T_k - 1.6722 \times 10^{-4} T_k^2 - \frac{20565.7315}{T_k} - 142.741722 \ln T_k} \quad (48)$$

### Implementation of the Model

The model requires as input temperature, pH,  $P_{H_2S}$ , and the hydrodynamic parameters: in this case, the rotating cylinder diameter and the rotational velocity. The corrosion potential then can be calculated by solving the charge balance equation:

$$\sum i_a = \sum i_c \quad (49)$$

which here takes the form:

$$i_{Fe} = i_{H_2S} + i_{H^+} + i_{H_2O} \quad (50)$$

Once the corrosion potential is known, the corrosion current and rate can be found from the anodic current (or the sum of cathodic current) at the corrosion potential. The individual and total cathodic and anodic curves, and predicted potentiodynamic sweeps can be then readily generated.

### MODEL VALIDATION

Performance of the model was validated by comparing the predictions with experimental results described above.

#### Effect of $pH_2S$

Figure 10 shows that the predicted corrosion rates from the electrochemical model are in good agreement with experimental results, which suggests that the electrochemical model captured the main effects of  $H_2S$  corrosion of mild steel in the absence of iron sulfide layers.

Figures 11, 12, and 13 show cathodic and anodic polarization curves changing with  $H_2S$  concentration for the different pH aqueous environments. The model prediction captures successfully the anodic reaction change in the low-pH range (Figure 12, for pH 3) and the cathodic reaction change in high-pH environments (Figure 13, for pH 5) due to the additional cathodic reaction:  $H_2S$  reduction. Predicted potentiodynamic sweeps are in good agreement with experimental results for individual reactions generated with the present model.

Using this kind of model, the cathodic polarization curves can be deconvoluted to show the contribution from three individual cathodic reactions ( $H^+$  reduction,  $H_2S$  reduction, and  $H_2O$  reduction). It can be seen, for example, that when increasing the  $H_2S$  concentration, the  $H^+$  reduction does not change, that the  $H_2S$  reduction curve moves to the higher values of the current (on the right of the graph) and that the  $H_2O$  reduction changes only a little (Figures 11, 12, and 13).

#### Effect of Flow Rate

The effect of flow rate on both cathodic reaction and anodic reaction at 1%(v) and 10%(v)  $H_2S(g)$  is depicted in Figures 14 and 15. Increasing rotating speed does not affect the anodic reaction and  $H_2O$  reduction, but accelerates the cathodic reaction as a result of the increase of mass-transfer-limiting current related to  $H^+$  reduction and  $H_2S$  reduction. Except for the case of the limiting current density at 200 rpm rotating

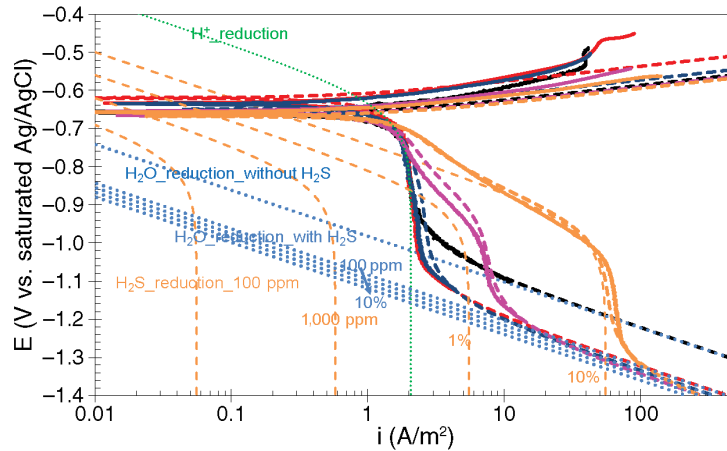


**FIGURE 11.** Comparison of predicted polarization curves with experimental results at different  $H_2S$  concentrations, pH 4, total pressure = 1.0 bar, 1,000 rpm, 30°C. Solid line: experimental curves. Dashed line: predicted curves. Black: 0 ppm(v)  $H_2S(g)$ , red: 100 ppm(v)  $H_2S(g)$ , dark blue: 1,000 ppm(v)  $H_2S(g)$ , pink: 1%(v)  $H_2S(g)$ , purple: 10%(v)  $H_2S(g)$ .

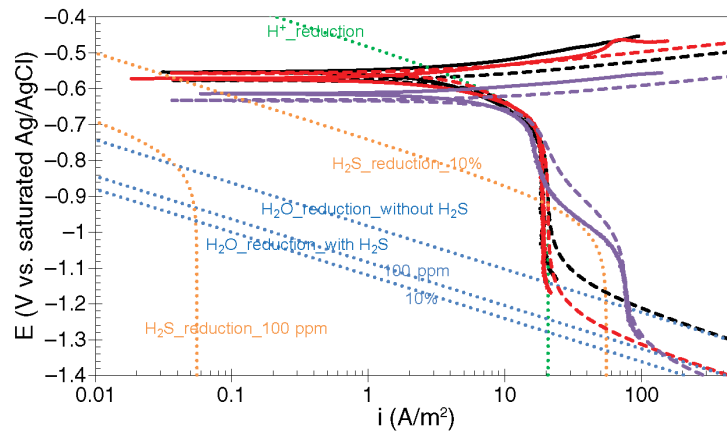


**FIGURE 12.** Comparison of predicted polarization curves sweeps with experimental results at different  $H_2S$  concentrations, pH 3, total pressure = 1.0 bar, 1,000 rpm, 30°C. Solid line: experimental curves. Dashed line: predicted curves. Black: 0 ppm(v)  $H_2S(g)$ , red: 100 ppm(v)  $H_2S(g)$ , purple: 10%(v)  $H_2S(g)$ .

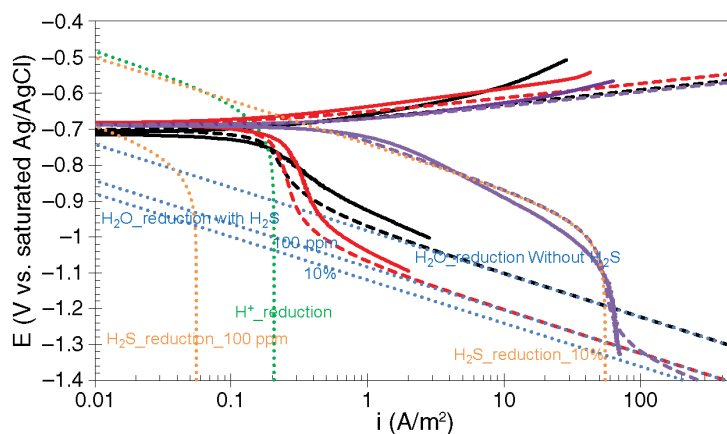


**FIGURE 13.** Comparison of predicted polarization curves with experimental results at different  $H_2S$  concentrations, pH 5, total pressure = 1.0 bar, 1,000 rpm, 30°C. Solid line: experimental curves. Dashed line: predicted curves. Black: 0 ppm(v)  $H_2S(g)$ , red: 100 ppm(v)  $H_2S(g)$ , purple: 10%(v)  $H_2S(g)$ .

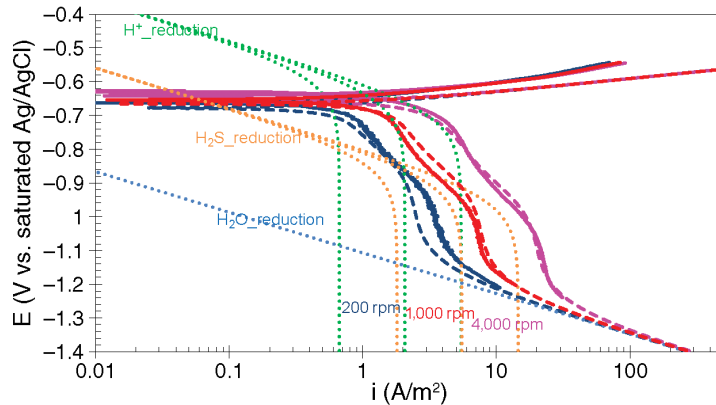


**FIGURE 14.** Comparison of predicted polarization curves with experimental results at different rotated speeds, pH 4, 1%(v)  $H_2S(g)$ , total pressure = 1.0 bar, 30°C. Solid line: experimental curves. Dashed line: predicted curves. Dark: 200 rpm, red: 1,000 rpm, pink: 4,000 rpm.

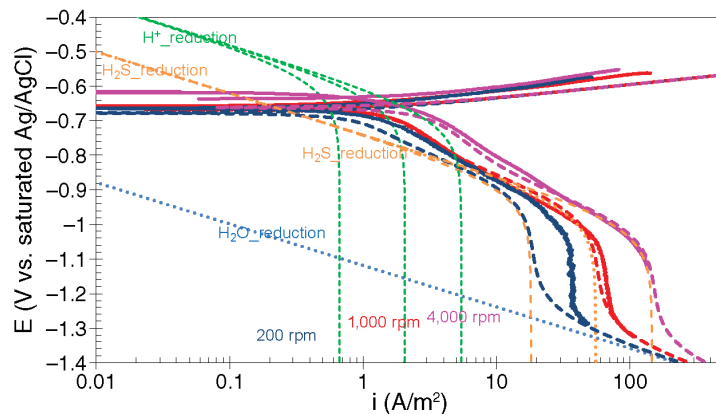


**FIGURE 15.** Comparison of predicted polarization curves with experimental results at different rotated speeds, pH 4, 10%(v)  $H_2S(g)$ , total pressure = 1.0 bar, 30°C. Solid line: experimental curves. Dashed line: predicted curves. Dark blue: 200 rpm, red: 1,000 rpm, pink: 4,000 rpm.

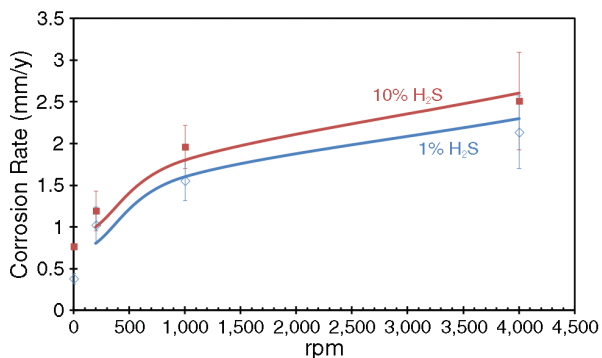


**FIGURE 16.** Comparison of predicted corrosion rate with LPR experimental results at different rotational speed, pH 4, total pressure = 1.0 bar, 30°C, points: experimental results, solid lines: predicted curves,  $B = 23$  mV/decade.

speed, all the predicted polarization curves agree well with the experimental results. Corrosion rate predictions are shown in Figure 16. The predicted corrosion rates are close to the experimental results.

### Effect of pH

Comparison between predicted polarization curves and experimental polarization curves in solution without  $H_2S$  are shown in Figure 17. A good agreement is found at each pH. From Figure 17,  $H^+$  reduction curves shift to the higher current values on the right with pH decrease, while anodic reaction curves move to lower values on the left with pH decrease.

When 100 ppm(v)  $H_2S(g)$  is present, the prediction of polarization curves is shown in Figure 18. Because of the low concentration of  $H_2S$  in solution, no obvious effect on the cathodic polarization curve is observed. As mentioned previously, anodic reaction is related to the  $HS^-$  concentration. At the same gas concentration of  $H_2S$ ,  $[HS^-]$  is inversely proportional to the pH, so the anodic reaction rate increases with pH increase. The experimental and predicted polarization curves were found to be in very good agreement.

For 10%(v)  $H_2S(g)$  present, the comparison of the predicted polarization curves with the experimental results is shown in Figure 19. It is evident that the

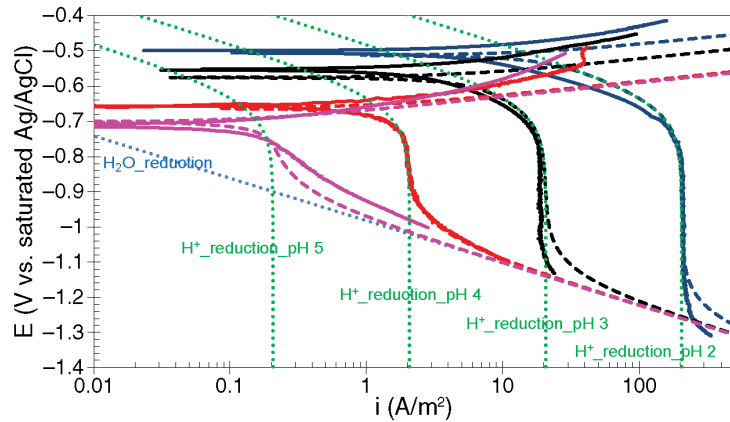


**FIGURE 17.** Comparison of predicted polarization curves with experimental results at different pH, 1,000 rpm, 0 ppm(v)  $H_2S(g)$ , total pressure = 1.0 bar, 30°C. Solid line: experimental curves. Dashed line: predicted curves. Pink: pH 5, dark blue: pH 2, black: pH 3, red: pH 4, pink: pH 5.

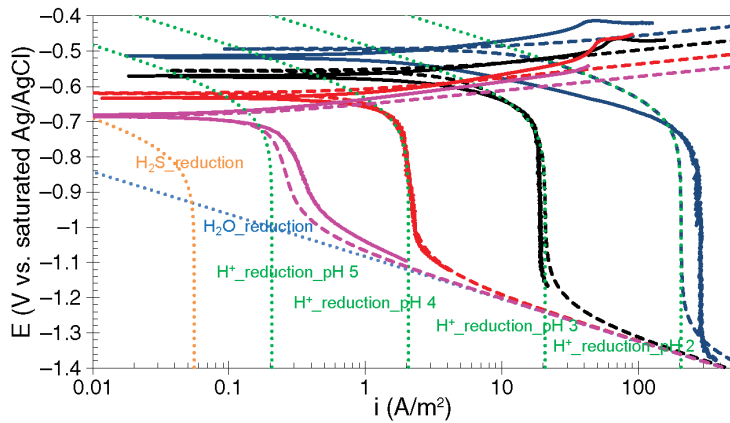


**FIGURE 18.** Comparison of predicted polarization curves with experimental results at different pH, 1,000 rpm, 100 ppm(v)  $H_2S(g)$ , total pressure = 1.0 bar, 30°C. Solid line: experimental curves. Dashed line: predicted curves. Pink: pH 5, dark blue: pH 2, black: pH 3, red: pH 4, pink: pH 5.

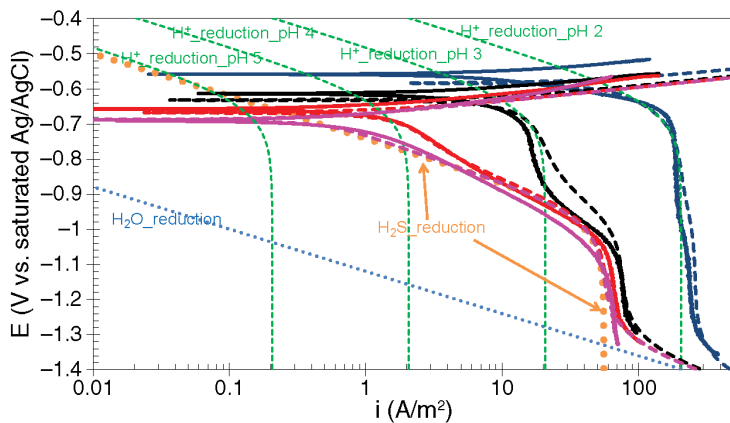


**FIGURE 19.** Comparison of predicted polarization curves with experimental results at different pH, 1,000 rpm, 10% (v)  $H_2S(g)$ , total pressure = 1.0 bar, 30°C. Solid line: experimental curves. Dashed line: predicted curves. Pink: pH 5, dark blue: pH 2, black: pH 3, red: pH 4, pink: pH 5.

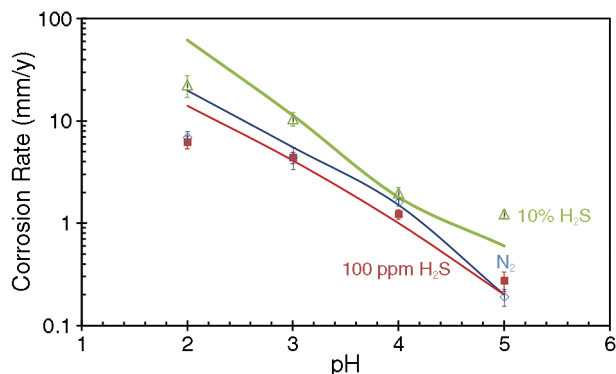


**FIGURE 20.** Comparison of predicted corrosion rate with experimental results at different pH, different  $H_2S$  concentrations, 1,000 rpm, total pressure = 1.0 bar, 30°C, point: experimental results, solid line: predicted curves. LPR constant  $B = 23$  mV/decade.

model prediction is in good agreement with the experimental data at each pH. When the  $H_2S$  concentration is higher, the  $H_2S$  reduction affects the overall cathodic polarization curves significantly. Anodic polarization curves are not sensitive to pH in Figure 19 because of the high concentration of  $HS^-$ .

Corrosion rate prediction at different pH is shown in Figure 20. The electrochemical model predictions are in good agreement with experimental results, which means the electrochemical model captured the main features of  $H_2S$  corrosion at different pH.

### Effect of Temperature

The effect of temperature on both cathodic reaction and anodic reaction at  $[H_2S] = 8.3 \times 10^{-4}$  M is depicted in Figure 21. Increasing temperature has a small influence on the anodic reaction, but accelerates the cathodic reaction greatly.  $H^+$  reduction,  $H_2S$  reduction, and  $H_2O$  reduction rate increase with temperature increase. All the predicted sweeps agree with experimental results well.

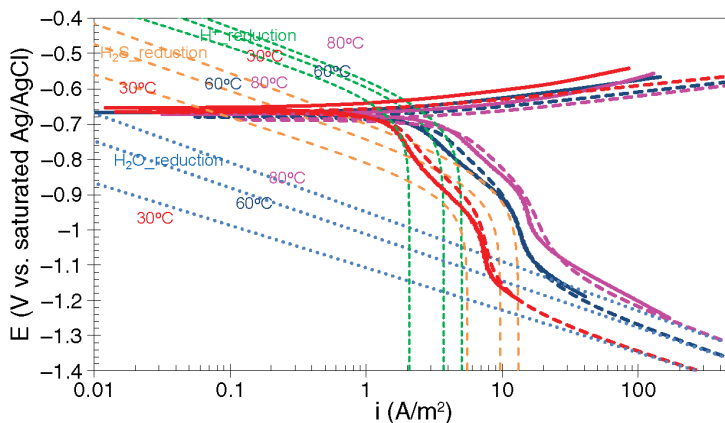


**FIGURE 21.** Comparison of predicted polarization curves with experimental results at different temperatures, 1,000 rpm,  $[H_2S] = 8.3 \times 10^{-4}$  mol/L, total pressure = 1.0 bar, 30°C. Solid line: experimental curves. Dashed line: predicted curves. Red: 30°C, dark blue: 60°C, pink: 80°C.

Corrosion rate predictions are shown in Figure 22. This electrochemical model captures well the corrosion rate change with temperature.

## CONCLUSIONS

- ❖ During aqueous corrosion of mild steel, the presence of dissolved  $H_2S$  in water affects both the cathodic reactions and the anodic reaction.
- ❖ An additional cathodic reaction, direct  $H_2S$  reduction, was clearly observed. This reaction is flow-sensitive and a mass-transfer-limiting current density was identified. The Tafel slope was observed to be close to 120 mV/decade at 30°C. The reaction order with  $C_{H_2S}$  is estimated to be close to 0.5.
- ❖ A retardation of  $H_2O$  reduction in the presence of  $H_2S$  was observed at all experimental conditions, even at pH 2.
- ❖ In different pH ranges, either acceleration or retardation of anodic dissolution of iron was seen in the presence of  $H_2S$  in acidic solutions. This effect is related to the chemisorption of  $HS^-$  ions. The effect can be explained by using the Langmuir adsorption model. The Tafel slope for the anodic dissolution of iron was 40 mV/decade ~ 50 mV/decade. When  $[HS^-]$  reached a saturation value, the anodic reaction current reached a maximum and became independent of both  $[HS^-]$  and pH.
- ❖ A new electrochemical model has been developed that can be used to simulate the effect of  $pH_2S$ , flow, temperature, and pH on corrosion of mild steel in an  $H_2S$  environment in the absence of iron sulfide layers.

## ACKNOWLEDGMENTS

The authors would like to express sincere appreciation to the following industrial sponsors for their financial support and direction: BG Group, BP,

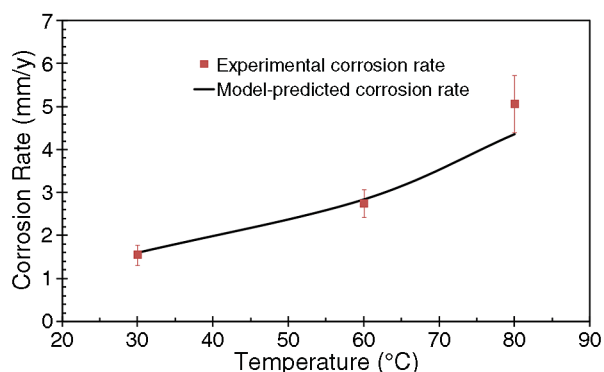


**FIGURE 22.** Comparison of predicted corrosion rate with experimental results at different temperatures, 1,000 rpm,  $[H_2S] = 8.3 \times 10^{-4}$  mol/L, total pressure = 1.0 bar, 30°C, Point: experimental results, solid line: predicted curves. LPR constant  $B = 23$  mV/decade.

Champion Technologies, Chevron, Clariant Oil Services, ConocoPhillips, Encana, ENI S.P.A., ExxonMobil, WGIM, NALCO Energy Services, Occidental Oil Company, Petrobras, PETRONAS, PTT, Saudi Aramco, INPEX Corporation, Total, and TransCanada.

#### REFERENCES

1. S.N. Smith, M.W. Joosten, "Corrosion of Carbon Steel by  $H_2S$  in  $CO_2$  Containing Oilfield Environments," CORROSION/2006, paper no. 06115 (Houston, TX: NACE International, 2006).
2. D.W. Shoesmith, P. Taylor, M.G. Bailey, D.G. Owen, *J. Electrochem. Soc.* 127, 5 (1980): p. 1007-1015.
3. W. Sun, "Kinetics of Iron Carbonate and Iron Sulfide Scale Formation in Carbon Dioxide/Hydrogen Sulfide Corrosion" (Ph.D. diss., Ohio University, 2006).
4. R.H. Hausler, "Contribution to the Understanding of  $H_2S$  Corrosion," CORROSION/2004, paper no. 04732 (Houston, TX: NACE, 2004).
5. S.N. Smith, J.L. Pacheco, "Prediction of Corrosion in Slightly Sour Environments," CORROSION/2002, paper no. 02241 (Houston, TX: NACE, 2002).
6. S.N. Smith, "A Proposed Mechanism for Corrosion in Slightly Sour Oil and Gas Production," 12th Int. Corrosion Congress: Corrosion Control for Low-Cost Reliability Conference, paper no. 385 (Houston, TX: NACE, 1993).
7. D.R. Morris, L.P. Sampaleanu, D.N. Veysey, *J. Electrochem. Soc.* 127, 6 (1980): p. 1228-1235.
8. Z.A. Iofa, V.V. Batrakov, Cho-Ngok-Ba, *Electrochim. Acta* 9, 12 (1964): p. 1645-1653.
9. X.L. Cheng, H.Y. Ma, J.P. Zhang, X. Chen, S.H. Chen, H.Q. Yang, *Corrosion* 54, 5 (1998): p. 369-376.
10. W. Sun, S. Nešić, *Corrosion* 65, 5 (2009): p. 291-307.
11. M. Eisenberg, C.W. Tobias, C.R. Wilke, *J. Electrochem. Soc.* 101, 6 (1954): p. 306-320.
12. S. Nešić, J. Postlethwaite, S. Olsen, *Corrosion* 52, 4 (1996): p. 280-294.
13. J.O. Bockris, D. Drazic, A.R. Despic, *Electrochim. Acta* 4, 2-4 (1961): p. 325-361.
14. D. Rickard, G.W. Luther, *Chem. Rev.* 107, 2 (2007): p. 514-562.
15. H. Ma, X. Cheng, G. Li, S. Chen, Z. Quan, S. Zhao, L. Niu, *Corros. Sci.* 42, 10 (2000): p. 1669-1683.
16. M. Nordsveen, S. Nešić, N. Nyborg, A. Stangeland, *Corrosion* 59, 5 (2003): p. 433-456.
17. P.W. Atkins (ed.), *Physical Chemistry*, 2nd ed. (Oxford, England: Oxford University Press, 1982).
18. R.C. Weast (ed.), *Handbook of Chemistry & Physics*, 66th ed. (Boca Raton, FL: CRC Press Inc., 1985).
19. J. Kittel, F. Ropital, F. Grosjean, E.M.M. Sutter, B. Tribollet, *Corros. Sci.* 66 (2013): p. 324-329.
20. R.H. Perry, D.W. Green, J.O. Maloney, *Perry's Chemical Engineers' Handbook* (New York: McGraw-Hill, 1984).
21. O.M. Suleimenov, R.E. Krupp, *Geochim. Cosmochim. Acta* 58, 11 (1994): p. 2433-2444.
22. Y.K. Kharaka, W.D. Gunter, P.K. Aggarwal, E.H. Perkins, J.D. Dedraal, United States Geological Survey Water-Resources Investigation Report, 1988, p. 88-4227.
23. O.M. Suleimenov, T.M. Seward, *Geochim. Cosmochim. Acta* 61, 24 (1997): p. 5187-5198.